Effects of Lower Hybrid Fast Electron Populations on Electron Temperature Measurements at JET

C P Tanzi[1], D V Bartlett, G J Kramer[1], B Schunke.

JET Joint Undertaking, Abingdon, Oxon, OX14 3EA.
[1] FOM Instituut voor Plasmafysica "Rijnhuizen', The Netherlands.

EFFECTS OF LOWER HYBRID FAST ELECTRON POPULATIONS ON ELECTRON TEMPERATURE MEASUREMENTS AT JET

C.P. TANZI(*), D.V. BARTLETT, G.J. KRAMER(*), B. SCHUNKE
JET Joint Undertaking, Abingdon OXON OX14 3EA UK
(*)FOM Instituut voor Plasmafysica "Rijnhuizen", The Netherlands

Abstract

The Lower Hybrid Current Drive (LHCD) system on JET has to date achieved up to 1.5 MA of driven current. This current is carried by a fast electron population with energies more than ten times the electron temperature and density about 10^{-4} of the bulk plasma. This paper discusses the effects of this fast electron population on our ability to make reliable temperature measurements using ECE and reviews the effects on other plasma diagnostics which rely on ECE temperature measurements for their interpretation.

1 Introduction

ECE electron temperature (T_e) measurements at JET are made with antennas on the outboard side of the tokamak. X-mode radiation is detected by a Michelson interferometer and a twelve channel grating polychromator, while a forty-four channel heterodyne radiometer measures either in the X-mode or O-mode. Most of the results presented in this paper are from the Michelson interferometer. It is absolutely calibrated, with an estimated systematic uncertainty of $\pm 10\%$, and has a spectral resolution of 15 GHz, corresponding to a spatial resolution of ~ 0.15 m. Its temporal resolution is 15 ms. The grating polychromator measures at twelve fixed frequencies and has a faster temporal resolution (10 μs) and is cross-calibrated against the Michelson interferometer. The heterodyne radiometer is described in Bartlett, 1992.

ECE T_e measurements at JET use the optically thick second harmonic X-mode. In thermal plasmas, overlap of the third harmonic limits the innermost radius for T_e measurements to about the plasma centre. On the outboard side, the first and second harmonics are overlapped at about the plasma edge. Frequencies in the first harmonic range encounter a non-propagating region formed by the upper hybrid resonance and the upper cut-off. This region lies between the first and second harmonics, as shown in figure 1.

In this paper, we use thermal emission and thermal resonance to refer to phenomena associated with the Maxwellian (thermal) electron population. Non-thermal emission is used to refer to the emission by the LHCD generated electrons.

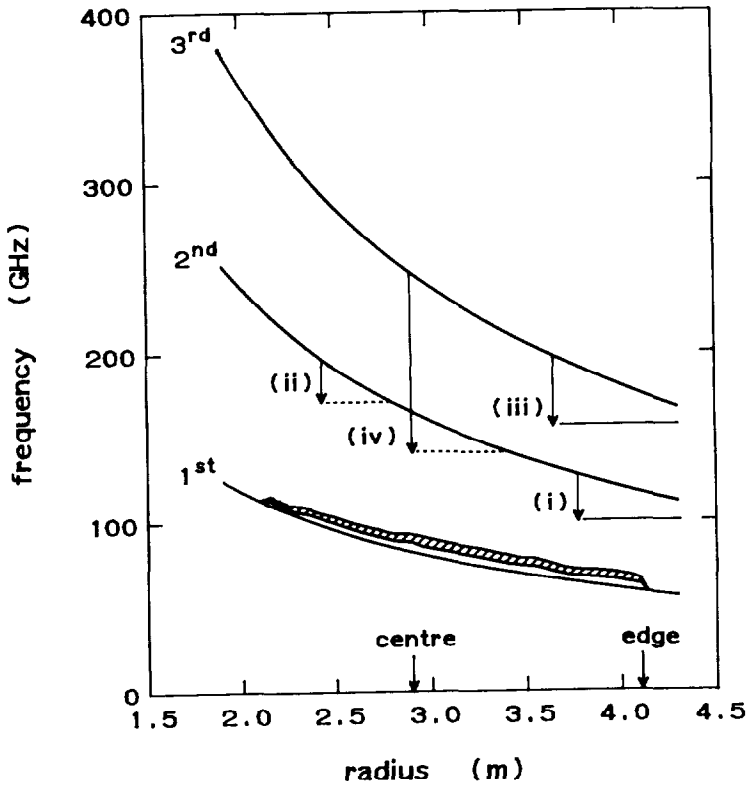

Fig.1 *Schematic showing frequency versus radius for the electron cyclotron resonances, and the non-propagating region between the upper cut-off and the upper hybrid resonance for the X-mode. Four different cases of downshifted emission by fast electrons are indicated: (i) downshifted second harmonic emission which propagates to the antenna (solid line), (ii) downshifted second harmonic emission which is reabsorbed by the second harmonic thermal resonance (dashed line), (iii) downshifted third harmonic which reaches the antenna (solid line), and (iv) third harmonic with a large downshift which is reabsorbed by the second harmonic thermal resonance (dashed line). It is the emission of case (iii) which may perturb ECE T_e measurements.*

For the energy range of the Lower Hybrid (LH) generated fast electrons (50-150 keV), the frequency of emission is subject to a significant relativistic downshift:

$$\omega = \frac{n\,\omega_{ce}}{\gamma(1-\beta_{\parallel}\cos\theta)}, \qquad \omega_{ce} = \frac{e\,B(R)}{m_0}, \qquad n = 1, 2, 3\ldots, \tag{1}$$

where e is the electron charge, m_0 the electron rest mass, R the tokamak major radius, $\gamma^2 = (1-\beta^2)^{-1}$, $\beta = v/c$, c is the speed of light, $v_{\parallel}$ the velocity component along the magnetic field and θ is the angle between the line of sight and the magnetic field. The antennas are oriented so that $\theta \simeq 90^0$.

Figure 1 also illustrates four different cases of downshifted emission which are relevant to the part of the spectrum used for T_e measurements. In case (i) the second harmonic downshifted emission can propagate to the antenna because the downshift changes the frequency to one which is not re-absorbed by the thermal component of the plasma, whereas in case (ii) the same downshift of emission at a smaller major radius results in reabsorption by the second harmonic thermal resonance. In case (iii) the downshifted third harmonic reaches the antenna because the strongly absorbing second harmonic thermal resonance is located behind it. When the downshift is large, as in case (iv), reabsorption by the thermal second harmonic again prevents the radiation from escaping. The downshifted emission of cases (i), (ii) and (iv) does not affect our second harmonic temperature measurements (although case (i) can be used to investigate the fast electron population, Ramponi 1992). It is the emission by the electrons of case (iii) which may perturb ECE T_e measurements.

The purpose of this paper is to determine to what extent the ECE T_e measurements in the core plasma are affected by emission from the fast electrons generated by LH power, and to review the consequences of this emission on other diagnostics whose interpretation relies on ECE T_e measurements.

2 Qualitative explanation of ECE behaviour during LHCD

Recalling that the kinetic energy $K = m_0c^2(\gamma^2 - 1)$, and using a vacuum magnetic field profile, $B(R) = B_0R_0/R$, where $B_0 = B(R_0)$, the emission at a fixed frequency ω in harmonic n can come from electrons at any radius R with energy K satisfying

$$R = n\, e\, m_0\, B_0\, R_0 \frac{511}{\omega\,(511 + K)}, \qquad n = 1, 2, 3\ldots, \qquad (K \text{ in keV}), \tag{2}$$

as shown in figure 2. Each of the curves on this figure corresponds to a fixed emission frequency. The upper three curves show the radii where downshifted third harmonic is emitted, as a function of electron energy. The three lower curves are the downshifted second harmonic radii for the same frequencies. The horizontal lines show the radii where the thermal electrons emit in the second harmonic for these frequencies. Downshifted third harmonic from high energy electrons, which is emitted from radii inboard of the thermal second harmonic radii, will be re-absorbed and not seen by antennas viewing the plasma from the outboard side. There is therefore an upper energy limit for the observed downshifted third harmonic, as shown by the vertical line.

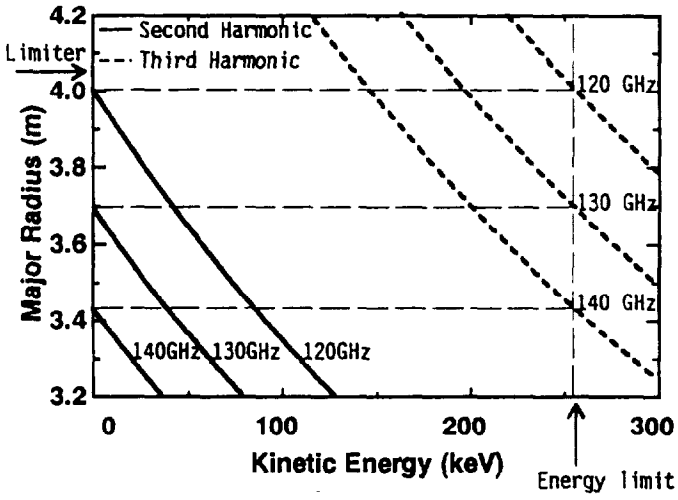

Fig.2 *Radius versus energy curves for three fixed frequencies. The three curves on the upper right correspond to downshifted third harmonic emission, while those on the lower left are for downshifted second harmonic. The corresponding thermal second harmonic radii are shown as horizontal lines. The upper energy limit for which third harmonic emission can be seen is the intersection of the horizontal lines with the third harmonic resonances.*

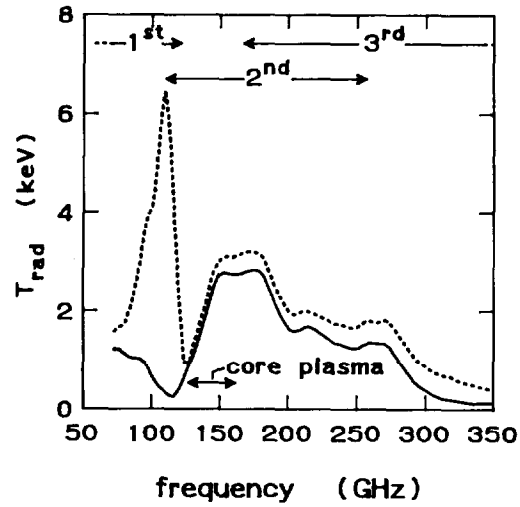

Fig.3 *Radiation temperature spectra measured by the Michelson interferometer before (solid line) and during (dashed line) a LH pulse. The frequency range of the first few (thermal) harmonics is indicated. The low frequency region of the spectrum corresponds to case (i) of figure 1.*

Radiation temperature spectra measured by the Michelson interferometer before and during a Lower Hybrid pulse are shown in figure 3. The spectrum shows clearly the effect of the fast electron population, but is quite different to that observed in the runaway regime where intense emission is seen across the whole frequency range (Costley, 1974). This is explained by our expectation of a fast electron population with limited energy range (50 to 150 keV) and low density ($\simeq 10^{-4}$ of the bulk plasma). The low frequency region of the spectrum, corresponding to cases (i) of figure 1 shows a strong non-thermal perturbation, with little emission from the thermal first harmonic reaching the antenna. At higher frequencies, where the thermal second harmonic resonance enters the plasma edge and rapidly becomes optically thick, the non-thermal feature experiences a sharp cut-off due to re-absorption.

The spectral region where the thermal second harmonic is optically thick is not significantly modified by the non-thermal emission of the fast electrons. As shown above, the non-thermal contribution at these frequencies is downshifted third harmonic, which is emitted by fast electrons between the thermal second harmonic layer and the antenna. Since this non-thermal emission is weak (radiation temperature $\leq$ 400 eV, see figure 3), relative to the black-body level for the fast electrons, it must be optically thin. The fast electrons therefore re-absorb very little of the thermal second harmonic radiation, and for this part of the spectrum we can treat the emission by the fast electrons as a perturbation added to the thermal emission:

$$T_{\mathrm{RAD}}(\mathrm{ECE}) \simeq T_2 + T_{\mathrm{RAD}}(\text{non-thermal}), \tag{3}$$

where $T_{\mathrm{RAD}}(\mathrm{ECE})$ is the total emission, T_2 is the thermal second harmonic emission ($T_2 = T_e$) and $T_{\mathrm{RAD}}(\mathrm{non-thermal})$ is the emission of the fast electrons.

3 LH power modulation measurements

As a first step to determine whether or not the non-thermal perturbation in equation (3) is significant (in relation to T_e or the change in T_e due to heating by the LH power), we examine some measurements made by the grating polychromator during LH power modulation experiments. Figure 4 shows the results of such a measurement. Below the LH power waveform (top trace) is shown the output of a polychromator channel measuring at a frequency just below the thermal second harmonic at the plasma edge, i.e. in the region where downshifted emission from the fast electrons dominates. The signal level increases by a factor of two when the LH power is on. The next trace is the signal from a polychromator channel measuring at a frequency corresponding to the plasma centre for the thermal emission. It also shows a substantial increase during the injection of LH power. Since the variation in other plasma parameters is small, it is possible to determine whether or not this increase is due solely to a temperature rise by comparing the apparent rate of rise of electron energy with the level of injected power. The fourth trace on figure 4 shows the apparent electron energy $W_e \equiv \int T_{\mathrm{RAD}}\, n_e\, dV$ (where the integration is made over the whole plasma volume) and the bottom trace compares the time derivative of this quantity with the Lower Hybrid power waveform. The maximum $dW_e/dt \simeq 1.2 \pm 0.2$ MJ/s is greater than the LH power $\simeq 0.8$ MW, showing that there is an overestimate of $\simeq 20\%$ during both switch-on and switch-off of the

Lower Hybrid power. It follows that, at least during the transient effect of the switch-on and off of LH power, the ECE signal cannot be entirely attributed to a temperature increase. In order to quantify this effect, we compare ECE and LIDAR measurements in steady state.

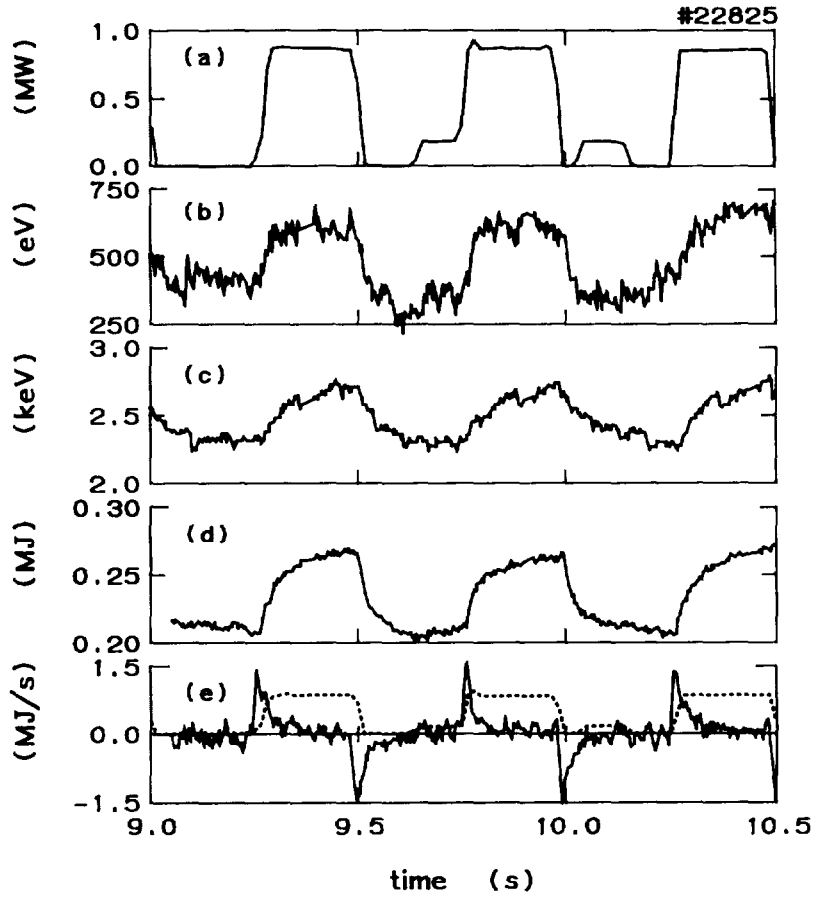

Fig.4 *Data obtained during LH power modulation. Trace (a) is the LH power. Trace (b) and (c) are the signals from two polychromator channels measuring at frequencies for which the thermal second harmonic resonance is just outside the plasma, and at the plasma centre. Trace (d) shows the apparent total electron stored energy calculated from the ECE and electron density signals, while trace (e) compares the time derivative of this energy (solid line) with the LH power waveform (dashed line).*

4 Determination of the non-thermal perturbation by comparison with LIDAR

The LIDAR (Light Detection And Ranging) Thomson scattering diagnostic (Salzmann, 1988) combines the Thomson back-scattering process with the LIDAR time-of-flight method to measure radially resolved T_e profiles. A short (300 psec) ruby laser pulse traverses the plasma along the major radius in the mid-plane. The spectrum of light backscattered by the electrons is recorded as a function of time as the light crosses the plasma, and analysed in the usual way to give T_e. The spatial resolution, determined by the duration of the laser pulse and by the response time of the detection system, is about 0.1 m, while photon statistics give rise to a random error on the T_e values which is typically 7% of the central electron temperature (T_{e_o}).

Fast electrons of energy greater than about 50 keV contribute only to the far wings of the Thomson scattered spectrum, which in the case of the LIDAR diagnostic on JET are outside the detection channels of the spectrometer. Moreover, because the fast electron density is low ($\simeq 10^{-4}$ of the thermal plasma density), their contribution to the scattered spectrum is below the LIDAR detection limit. Hence, it should be possible to determine the perturbation of the ECE radiation temperature during LHCD by using the LIDAR measurement of T_e in

equation (3):

$$T_{\mathrm{RAD}}(\text{non-thermal}) = T_{\mathrm{RAD}}(\text{ECE}) - T_e(\text{LIDAR}). \quad (4)$$

There are two difficulties with this analysis. Both the random error of the LIDAR measurements and the systematic uncertainty of the ECE measurements may be larger than the non-thermal perturbation. To overcome the LIDAR statisical errors, the comparison is made for a large number of measurements. To overcome the problem of a possible systematic difference between the two diagnostics, the ECE and LIDAR are compared in thermal plasmas (i.e. without Lower Hybrid) to obtain a correction factor, κ. The T_{RAD}(ECE) emission of equation 4 is therefore the measured emission scaled by the factor κ. It should be noted that for this analysis, it is a matter of convenience that the ECE values are scaled to agree with LIDAR, rather than the reverse. The values of κ are always close to unity ($\kappa \simeq 0.9$), so that in this analysis (which has uncertainties much larger than 10%) it makes no practical difference which diagnostic is assumed to have the systematic error. To minimize any spurious effects due to the slightly different sightlines of the two diagnostics, the different radial resolutions and uncertainty in the radial position of the ECE profile (due to the uncertainty in the calculation of the magnetic field), the profiles are averaged over a radial interval of 0.2 m. The calculation is made at six radial positions, from 2.8 m to 4.0 m.

The limited quantity of data which is available does not allow the analysis to be made separately for many different plasma regimes. For example, Ion Cyclotron Resonance Frequency (ICRF) heated plasmas have been excluded from this analysis, because of the large variety of input powers and the possible direct interaction of LH generated fast electrons with ICRF (Gormezano, 1991). The principal difference between the different plasmas used in this analysis is in the electron temperature, which varies with the level of LH power and other additional heating methods, but is also correlated with the electron density. The central density varies between $\approx 2.5\ 10^{19}$ to $\approx 3.5\ 10^{19}$ m^{-3} for these discharges.

Since LH current drive efficiency scales with T_e (Gormezano, 1992), the data have been subdivided into low ($T_{eo} < 3$ keV) and high ($T_{eo} > 3$ keV) temperature regimes. The high T_e pulses are also generally lower density. This subdivision has been dictated by the limited number of data available for this analysis, which does not allow a study of the density parameter as well. A direct comparison of the non-thermal perturbation for low and high T_e plasmas is therefore not possible.

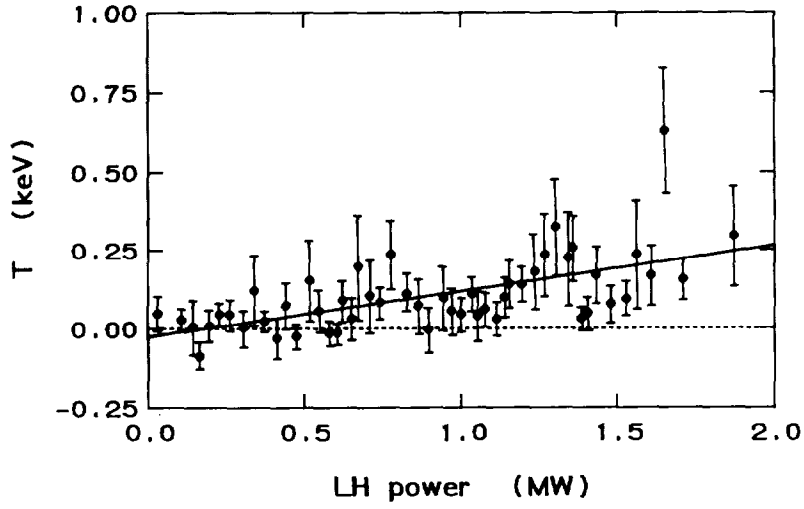

Fig.5 *Example of the analysis of the non-thermal perturbation of the ECE temperatures for low T_e plasmas, averaged over the radius range 2.8 to 3.0 m. The non-thermal perturbation is calculated according to equation 4 as a function of LH power. The measurements have been arranged in groups of 10 at the same LH power, the average value of each group and the standard error of the mean being plotted. The best fit straight line through the data is shown.*

Figure 5 is an example of this analysis for low T_e plasmas, over the radius range 2.8 to 3.0 m. It shows the non-thermal perturbation calculated according to equation 4 as a function of LH power. Approximately 500 profile measurements have been used. For ease of presentation, the measurements have been arranged in groups of 10 at the same LH power, the average value of each group being plotted. The scatter in the data is large. Although the non-thermal perturbation is probably a complex function of the Lower Hybrid power, the scatter allows us to use only a simple model:

$$T_{\mathrm{RAD}}(\text{non-thermal}) = \beta P(LH), \tag{5}$$

where the ECE measurements have been scaled by the correction factor κ defined above. The proportionality constant, β, is obtained by a least-squares fit on the data of figure 5. The result in this case is $\beta = 140 \pm 30$ eV/MW. The fit is not constrained to pass through the origin, but in fact is very close to doing so. This indicates that the cross-calibration of the ECE against the LIDAR for thermal plasmas has given an accurate result. In some instances, generally at the larger radii, the calculated intercept of the regression line is not so close to zero. This is taken into account in the quoted errors on values of β, but is not generally a large effect.

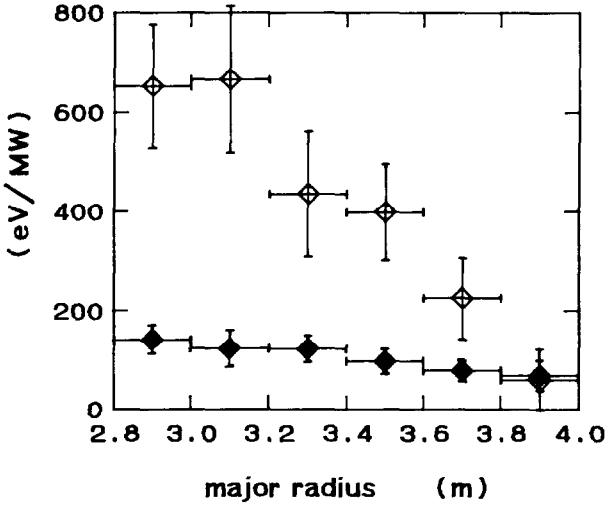

Fig.6 *Deduced values of β (equation 5) at six radial positions, from 2.8 m to 4.0 m, for $T_{eo} < 3\ keV$ (filled diamonds) and $T_{eo} > 3\ keV$ (open diamonds). The high T_e pulses are generally lower density. The horizontal bars represent the spatial averaging, the vertical bars are the esimated total error in the analysis.*

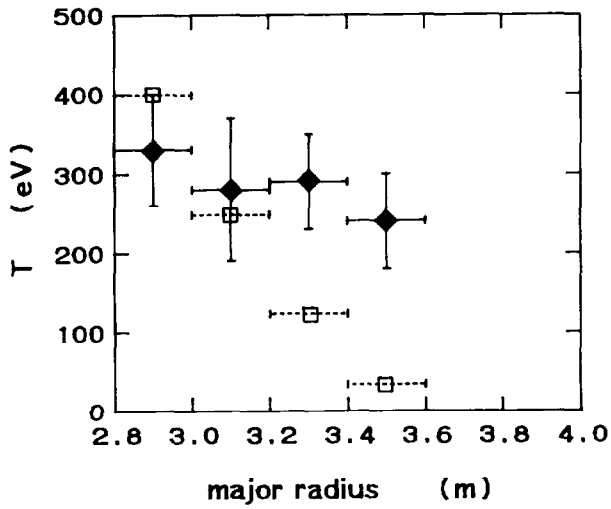

Fig.7 *Estimated non-thermal perturbation for a plasma (filled diamonds) with $T_{eo} \approx 1.4$ keV and 2 MW of LH power, using the β values of figure 6. The open squares are the result of a calculation with the ECLH code.*

Figure 6 shows the deduced non-thermal perturbations as a function of radius for low and high temperature plasmas. It can be seen that the LHCD indeed produces more non-thermal emission in high electron temperature plasmas. Moreover, the perturbation decreases with radius. This is due to the smaller number of fast electrons between the optically thick thermal second harmonic layer and the antenna when this layer is close to the outboard edge of the

plasma. The general conclusion is that at LH power levels up to 2 MW, the non-thermal perturbation of the ECE T_e is $\approx 5\%$ of T_e, but the errors in the analysis are too large to use this for routine correction of ECE in LH plasmas.

In figure 7 the data of figure 6 has been used to predict the non-thermal perturbation for a plasma with $T_{eo} \approx 3$ keV and 2 MW of LH power, and the result is compared with a simulation made using the ECLH code (Ramponi, 1992). For the simulation, some moments of the fast electron distribution function have been estimated by matching measured and calculated spectra in the low frequency region where the downshifted second harmonic emission dominates. The simulation and the experimentally determined values of β are consistent in the plasma core, but the agreement becomes poor near the edge. There are three possible causes of this effect. The first is that the spatial distribution of the fast electrons used in this simulation could be narrower than the actual spatial distribution in the plasmas used in this analysis. Alternatively, the relatively simple fast electron distribution function model used in the simulation (a single drifting Maxwellian which does not well represent the fast electron tail for energies of the order of the thermal energy) is likely to underestimate the contribution of the downshifted electrons for frequencies corresponding to the edge. The third possible explanation is that the ECLH code calculates strictly X-mode emission. However the JET ECE antennas are oriented to collect vertical polarization and therefore, because of the poloidal field, they also collect a small component (typically 5%) of the O-mode emission. Since the optical depth of the thermal second harmonic O-mode is small, there is no screening of non-thermal emission by the thermal component of the plasma and hence the O-mode non-thermal perturbation may not decrease much near the plasma edge.

Further simulations are required to investigate the relative importance of each of these possible explanations.

5 The effect of the perturbation on applications of T_e measurements

5.1 Edge T_e measurements

Edge T_e measurements in thermal plasmas are reliable provided the optical depth is greater than about 2 (Bartlett, 1990). However, it is clear from data such as that in figure 3 that in the presence of a fast electron population, much greater optical depth (> 4) is needed to screen the intense downshifted second harmonic emission. Unfortunately, the analysis summarized in figure 6 shows that near the plasma edge this condition is not sufficient and T_e measurements suffer a large perturbation, even though the optical depth is large. As discussed above, the cause of this is not certain. The data show that during LHCD T_e measurements typically have perturbations greater than 10% at radii greater than about 3.8 m (.35 m from the plasma edge) so that edge T_e measurements are not possible in these discharges.

5.2 Steady state absolute T_e measurements

The analysis of many different diagnostic measurements requires the absolute electron temperature and its spatial profile as input. In addition to the quantities related solely to the electrons (such as electron energy content, pressure profiles and thermal transport) the T_e profile is widely used in the analysis of spectroscopic data (eg for impurity profiles and

transport), neutron measurements etc. It is also required in a variety of plasma modelling calculations, such as neutral beam power deposition and pellet ablation. Moreover, since the outputs of these analyses are often linked together to synthesise an overall picture of plasma behaviour, the propagation of the error due to the non-thermal perturbation is very difficult to determine.

However, the non-thermal perturbation due to $\sim$ 1 MW of LH power is small, so that it may not cause a significant effect in the diagnostic analysis chain. A simple example is given in figure 8 where the behaviour of the effective ion charge number Z_{eff}, deduced from visible bremsstrahlung measurements, is shown during a LH power modulation experiment. Correcting the T_e profile using the result of the LIDAR comparisons results in only a small correction to the value of Z_{eff}. The modulation of Z_{eff} is therefore largely due in this case to the impurity influx associated with this level of LH power. At higher electron temperatures, and higher LH power levels, the perturbation of the measured T_e may have a more significant effect.

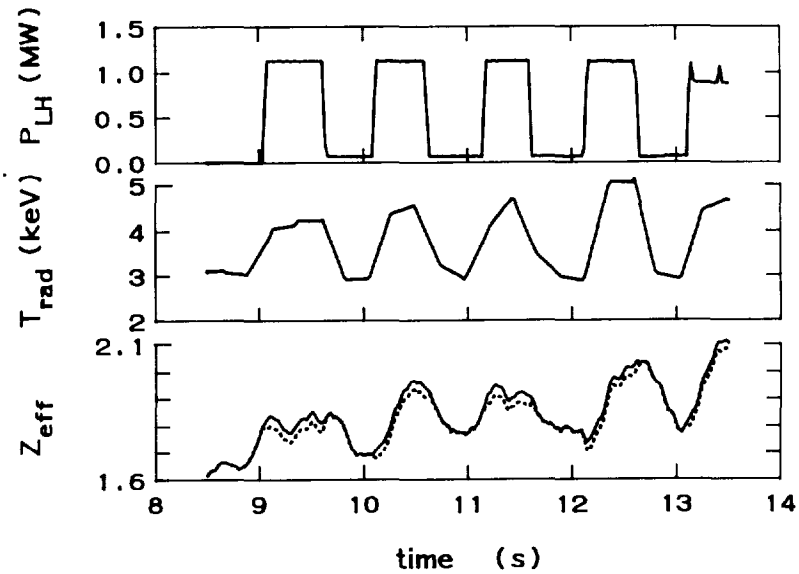

Fig.8 *The upper trace is the LH power modulation, the middle trace the Michelson Interferometer measurements used in the calculation of Z_{eff} from visible bremsstrahlung measurements (lower trace). The time scale evolution of Z_{eff} follows more closely the T_e measurement, with a very slow temporal resolution, than the Lower Hybrid switch-on and off. The dotted line shows the Z_{eff} signal corrected for the non-thermal perturbation.*

5.3 Transient T_e changes

When the ECE diagnostics are used to make measurements of transient, localized changes in T_e, valid results may be obtained in spite of the non-thermal perturbation. The reason is that fast electrons from the whole region between the thermal second harmonic layer and the plasma edge contribute to the non-thermal perturbation. Any localized change to the fast electron population will therefore have only a small effect on the total non-thermal emission level. In examining experimental data, a simple check is to look for substantial differences in the time evolution of the signals from neighbouring channels (i.e. over a small frequency range). Such differences must reflect local T_e changes, despite the presence of the non-thermal perturbation. Phenomena which are likely to give rise to localized T_e transients which can still be measured during LHCD include MHD oscillations, the sawtooth collapse and its associated heat pulse.

An example of this is shown in figure 9, which compares similar sawtooth collapses in two pulses. Both pulses have 2 MW of ICRF heating and the second pulse has, in addition,

1 MW of LH power. The figure shows the time evolution of ECE signals measured with the polychromator, both near the plasma centre and just outside the inversion radius. The time evolution of the signal is the same for the two pulses.

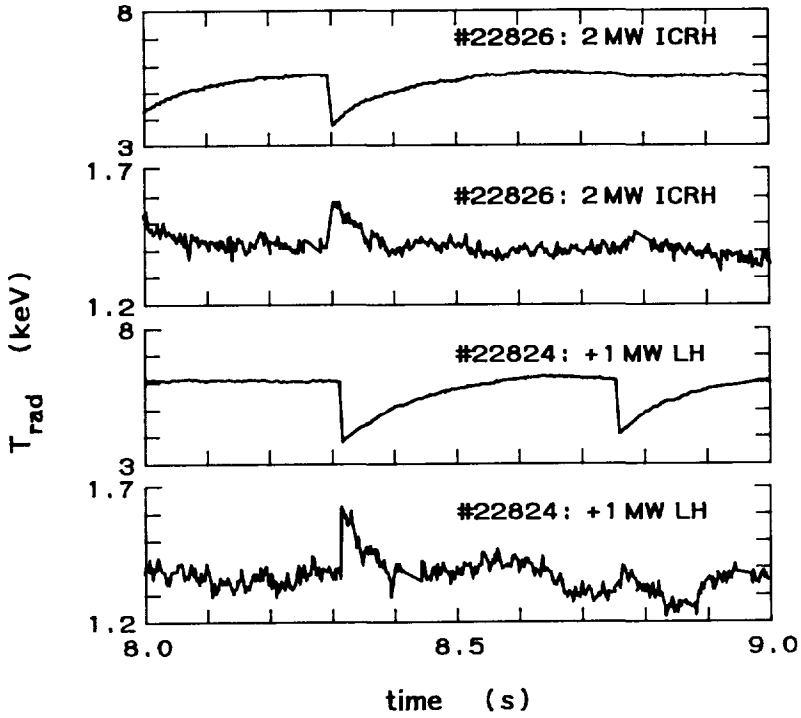

Fig.9 *Measurements with the polychromator for two similar pulses with 2 MW of ICRF heating. The lower traces are from a pulse which also has 1 MW of LH power. For each pulse, traces are shown for frequencies corresponding to the plasma core (upper trace) and to a similar distance from the inversion radius, close to the mixing radius (lower trace).*

6 Extrapolation of the non-thermal perturbation to higher LH power

The full JET LH system (Pain, 1989), which will increase the injected LH power from 2 MW to about 10 MW, is being installed during the present shutdown. To predict the effect of the higher power, the fast electron density has been scaled from the present results (Ramponi, 1992), assuming the same LHCD efficiency. Figure 10 shows the emission spectrum predicted by the ECLH code for a plasma with about 5 keV and 2 $10^{19}m^{-3}$ density in the centre, but with the fast electron density increased by a factor 13. The effect on the second harmonic region of the spectrum is now substantial, the perturbation being well above the systematic uncertainties in the ECE measurements.

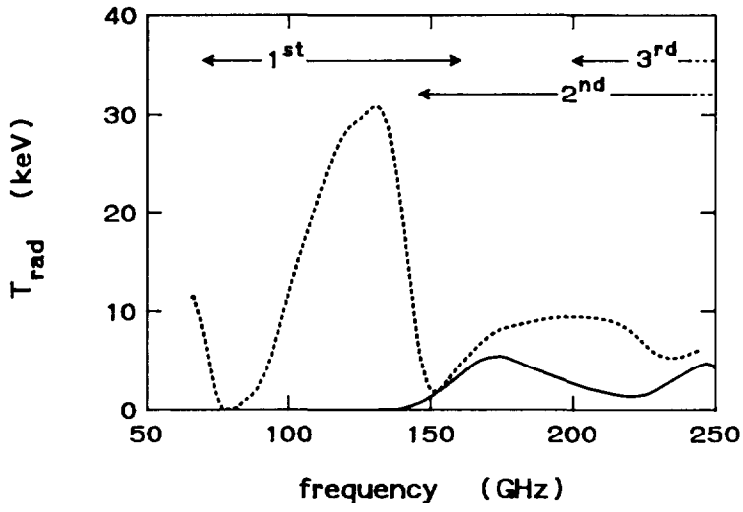

Fig.10 *Calculated emission spectrum of a plasma before (solid line) and during (dotted line) 10 MW of LH power. The frequency range of the first few (thermal) harmonics is indicated.*

The figure suggests that T_e measurements might still be possible in the region near the plasma edge where the optical depth is still large. However, the analysis above indicates that this will not occur, and that no reliable temperature measurements by ECE will be possible in these plasmas.

7 Conclusions

The behaviour of the non-thermal perturbation of the second harmonic X-mode ECE during LHCD experiments has been explained qualitatively and investigated experimentally. The perturbation is due to a low level of third harmonic emission by fast electrons spread across the region between the optically thick thermal second harmonic resonance and the ECE antennas on the outboard side of the plasma. By comparing with the temperatures measured by the LIDAR Thomson scattering diagnostic, the magnitude of the perurbation has been determined. Around the plasma centre, it varies from $\approx$ 140 eV/MW of injected LH power at low T_e and high density, up to 650 eV/MW for T_e above 3 keV and low density. Closer to the plasma edge, the corresponding values are 70 and 60 eV/MW. The perturbation near the plasma centre is consistent with code simulations, but exceeds the predictions near the edge. Several possible explanations of this discrepancy are still being investigated.

It is difficult to quantify how the non-thermal perturbation propagates through the interpretation of other diagnostic measurements which rely on ECE temperature profiles. In cases which have been investigated, the expected level of perturbation of the ECE is small so that there is little consequence for the other measurements. In the case of transient, localized changes to the electron temperature, the ECE measurements can still be used since the non-thermal perturbation always originates from a large range of major radius and is therefore little affected by the localized change.

We use the systematic uncertainty in the absolute spectral intensity measured by the Michelson interferometer ($\pm$10%) as the criterion for determining the significance of the non-thermal perturbation. In present experiments the perturbation is generally less than 5%, so the T_e data may still be used, with some reservations. Extrapolating the present results to the power levels expected when the full LHCD system is operational shows that perturbations well above the 10% level are expected, and ECE T_e measurements are likely to be unreliable.

Future work in this area will be aimed at exploring a wider range of plasma parameters, with a larger range of LH power levels. This may allow the dependence of the non-thermal perturbation on a number of plasma parameters, in particular the electron density and temperature and the LH power, to be more precisely quantified.

Acknowledgements

We would like to thank A. Airoldi and G. Ramponi for the useful discussions on the ECLH simulation code, P.D. Morgan and M.J. Loughlin for advice on the propagation of T_e errors in other diagnostics, H.J. de Blank for useful discussions on the statistical analysis, and M. Brusati for discussions on the JET Lower Hybrid system. Advice by A.E. Costley throughout the preparation of this manuscript is acknowledged. One of the authors (CPT) would like to thank JET Joint Undertaking for financial support during the execution of this work. Part of the work was performed under the Euratom-FOM Association agreement with financial support from NWO and Euratom.

References

Bartlett D.V. *et al.* (1990), Journal of Nuclear Materials 176-177, 1064 (1990).
Bartlett D.V. *et al.* (1992), "The upgraded JET ECE heterodyne radiometer and its application to fast phenomena", this conference.
Costley A.E. *et al.* (1974), Phys. Rev. Lett. **33**, 758.
Gormezano C. *et al.* (1991), Proc. of IAEA Tech. Comm. on Fast Wave Current Drive in Reactors, Arles 1991.
Gormezano C. and the JET team (1992), 14th IAEA Meeting, Würzburg 1992.
Pain M. *et al.*, Proc. 13th Symp. on Fusion Engineering, Knoxville USA 1989.
Ramponi G. *et al.* (1992), Proc. 19th European Conference on Controlled Fusion and Plasma Physics, Innsbruck 1992.
Salzmann H. *et al.* (1988), Rev. Sci. Instrum **59**, 1451 (1988).